BIOCHEMISTRY
including biophysical chemistry & molecular biology

Article

pubs.acs.org/biochemistry

Structure and Backbone Dynamics of Vanadate-Bound PRL-3: Comparison of ^{15}N Nuclear Magnetic Resonance Relaxation Profiles of Free and Vanadate-Bound PRL-3

Ki-Woong Jeong,[†] Dong-Il Kang,[†] Eunjung Lee,[†] Areum Shin,[†] Bonghwan Jin,[†] Young-Guen Park,[†] Chung-Kyoung Lee,[‡] Eun-Hee Kim,[‡] Young Ho Jeon,[§] Eunice Eunkyeong Kim,[∥] and Yangmee Kim*[,†]

[†]Department of Bioscience and Biotechnology and BioMolecular Informatics Center, Konkuk University, Seoul 143-701, South Korea

[‡]Magnetic Resonance Team, Korea Basic Science Institute, Ochang, Chungbuk 363-883, South Korea

[§]College of Pharmacy, Korea University, Jochiwon, Chungnam 339-700, South Korea

[∥]Life Sciences Division, Korea Institute of Science and Technology, Seoul 136-791, South Korea

ABSTRACT: Phosphatases of regenerating liver (PRLs) constitute a novel class of small, prenylated phosphatases with oncogenic activity. PRL-3 is particularly important in cancer metastasis and represents a potential therapeutic target. The flexibility of the WPD loop as well as the P-loop of protein tyrosine phosphatases is closely related to their catalytic activity. Using nuclear magnetic resonance spectroscopy, we studied the structure of vanadate-bound PRL-3, which was generated by addition of sodium orthovanadate to PRL-3. The WPD loop of free PRL-3 extended outside of the active site, forming an open conformation, whereas that of vanadate-bound PRL-3 was directed into the active site by a large movement, resulting in a closed conformation. We suggest that vanadate binding induced structural changes in the WPD loop, P-loop, helices α4−α6, and the polybasic region. Compared to free PRL-3, vanadate-bound PRL-3 has a longer α4 helix, where the catalytic R110 residue coordinates with vanadate in the active site. In addition, the hydrophobic cavity formed by helices α4−α6 with a depth of 14−15 Å can accommodate a farnesyl chain at the truncated prenylation motif of PRL-3, i.e., from R169 to M173. Conformational exchange data suggested that the WPD loop moves between open and closed conformations with a closing rate constant k_{close} of 7 s^{-1}. This intrinsic loop flexibility of PRL-3 may be related to their catalytic rate and may play a role in substrate recognition.

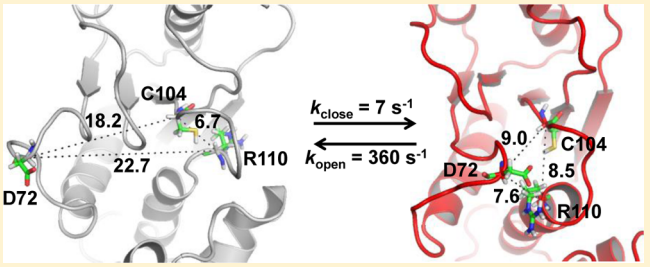

Phosphorylation and dephosphorylation are among the most important modifications by which biological systems control protein function to transduce information between distinct cellular sites.[1] The level of tyrosine phosphorylation is modulated by the combined action of protein tyrosine kinases and protein tyrosine phosphatases (PTPs).[2] Members of the family of phosphatases of regenerating liver (PRL) are unique in the PTP superfamily because of the CAAX prenylation motif at their C-termini. However, the cellular role of PRL enzymes has not yet been established.[3,4]

PRL-1, the first member of the PRL family to be discovered, was identified as a protein whose levels were increased in regenerating livers.[5,6] Two other PRLs, PRL-2 and PRL-3, were subsequently identified and found to be closely related to PRL-1 with regard to sequence and structure.[7−9] PRL-1 is primarily localized in the brain and muscle; PRL-2 is preferentially expressed in skeletal muscle, and PRL-3 is found specifically in cardiac and skeletal muscles.[9,10] In dividing cells, PRLs are located at the mitotic spindle, whereas they are membrane-associated in interphase cells. It is conceivable that the cell cycle-dependent localization confines PRL, limiting its access to substrates.[11]

PRL members have been linked to oncogenic events such as angiogenesis, cell invasion, motility, and metastasis,[12] and their proposed modes of action include stimulation of Src, Rho, or phosphoinositide 3-kinase (PI3K) signaling pathways.[13,14] To date, ezrin, a member of the ezrin/radixin/moesin (ERM) family,[15,16] elongation factor 2,[16] keratin 8,[17] integrin β1,[18] stathmin,[19] nucleolin,[20] phosphatidylinositol 4,5-bisphosphate, and repressor/activator protein 1[21] have been reported as putative substrates or binding partners of PRL-3.[22] The PRL-3 protein was also found to display a distinct expression pattern during gliomagenesis. PRL-3 is undetectable in normal brain tissue and grade I gliomas. However, grade II gliomas and high-grade glioma tissues display low and high PRL-3 levels, respectively.[23] Interestingly, PRL-3 levels correlate with the levels of several matrix metalloproteinases that are instrumental in the proteolytic degradation of the extracellular matrix, suggesting that PRL-3 is associated with glioma invasion.[11] Because of its high expression levels in metastatic tumors, PRL-

Received: March 29, 2014
Revised: June 28, 2014
Published: July 1, 2014

3 could be a molecular marker for evaluating the aggressiveness and prognosis of colorectal cancer and could serve as a novel therapeutic target for colorectal metastases.[12,24−29]

PTPs are characterized by the PTP signature motif CX_5R (P-loop) and a WPD active-site loop. These loops are central to the catalytic mechanism.[30,31] The phosphate group of phosphotyrosine (pTyr) is coordinated by the main-chain amide group and the arginine side chain of the P-loop, which places the phosphorus atom adjacent to the catalytic cysteine residue in the P-loop.[32] Structural analyses of several different PTPs revealed a conformational change in the WPD loop between the unliganded free form and the vanadate-bound form. The WPD loop in the active site of PTPs exhibits an open conformation in the free form; its catalytic aspartic acid residue is approximately 12 Å from the catalytic cysteine residue in the P-loop.[33] Opening of this loop is necessary for the release of the product and binding of new substrate.[33] In the ligand-bound, closed conformation, the WPD loop is shifted by as much as 10 Å to become positioned closely above the phenyl ring of pTyr, allowing the side chain of the catalytic aspartic acid residue to act as a general acid in the catalytic reaction.[30,34]

Solution structures of PRL-3, including one free form and one phosphate-bound form, have been determined using nuclear magnetic resonance (NMR) spectroscopy.[35,36] In free PRL-3, the flexibility of the P-loop comprising the active site causes resonances to disappear, and the number of nuclear Overhauser effects (NOEs) in this loop region is insufficient to determine its structure. Vanadate, which inhibits phosphatase-catalyzed phosphate ester hydrolysis, is commonly used to block the activity of PTPs.[37] Upon addition of sodium orthovanadate to free PRL-3, missing amide signals arising from this conformational flexibility appeared at residues near the active site.[35] These signals indicate that the binding of vanadate ions stabilizes these parts of PRL-3. In structures of free and phosphate-bound PRL-3s, the WPD loop has been reported to be in an open conformation.[35,36] However, the structure of vanadate-bound PRL-3, which may be in a closed conformation, has not yet been reported.

Changes in the protein conformation are essential for the enzymatic function, playing key roles in molecular recognition, rate-limiting conformational transitions, and catalysis. Because the time scales of these protein conformational motions vary widely, i.e., from picoseconds to seconds, solution NMR is a suitable technique for analyzing such motions.[38,39] Recently, active-site loop motions in YopH, a virulence factor from *Yersinia*, and PTP1B, a human phosphatase, have been addressed by Loria's group.[40] The NMR data showed that the phosphorylation levels can be modulated through control of WPD loop kinetics. Because the backbone dynamics of the complete sequences of free and vanadate-bound PRL-3s have not yet been studied, we used solution NMR techniques in this study to investigate the tertiary structure and active-site loop motions in vanadate-bound PRL-3.

METHODS

Expression and Purification of PRL-3. *Escherichia coli*-expressed PRL-3 was purified and labeled as described previously.[35] Briefly, the catalytic domain of human PRL-3 (amino acids 1−162) was cloned into the pET-21b vector (Novagen Inc., Madison, WI) and overexpressed in *E. coli* BL21(DE3) without tag or fusion sequences. Isotopically enriched PRL-3 was prepared from cells grown in M9 minimal medium containing [^{15}N]ammonium chloride and [^{13}C]-glucose (Cambridge Isotopes Laboratory, Andover, MA). The protein was purified by cation exchange chromatography followed by size-exclusion chromatography. The protein was exchanged into 50 mM 4-(2-hydroxyethyl)-1-piperazineethanesulfonic acid (HEPES), 100 mM NaCl, and 10 mM dithiothreitol (pH 7.3). Vanadate-bound PRL-3 was prepared by the addition of 3.0 mM sodium orthovanadate.

NMR Experiments. Samples of PRL-3 for NMR were prepared at a final concentration of 1.0 mM. The experiments were performed at 303 K on 800 and 600 MHz Bruker NMR spectrometers at the Korea Basic Science Institute (Ochang, Korea). Data sets were processed with NMRPipe[41] and interpreted with Sparky 3.1.[42] Structure calculations were performed with CYANA 2.1.[43] The main-chain C_α, H_α, N, and NH and side-chain C_β resonances were assigned using conventional heteronuclear HNCA, HN(CO)CA, HNCACB, CBCA(CO)NH, and HNHA experiments. The side-chain signal assignments were obtained using HCCH total correlation spectroscopy (HCCH-TOCSY), CCH-TOCSY, CC(CO)NH, and HCC(CO)NH. NOE distance constraints were measured from three-dimensional ^{1}H−^{15}N and ^{1}H−^{13}C nuclear Overhauser effect spectroscopy-heteronuclear single-quantum coherence (NOESY-HSQC) spectra acquired using mixing times of 100 and 120 ms.[35] Backbone torsion angle restraints were predicted from chemical shifts using TALOS+.[44] ^{15}N residual dipolar couplings (RDCs) were measured for the protein−detergent complex weakly aligned in a radially compressed polyacrylamide gel.[45] The chemical shifts, coordinates, and NMR-derived constraints have been deposited in the Biological Magnetic Resonance Bank (entry 19395 for PRL-3 in complex with vanadate).

Longitudinal (R_1) and transverse (R_2) relaxation and heteronuclear NOE (hNOE) NMR spectra were recorded. NMR spin-relaxation experiments were performed using published, gradient-selected, sensitivity-enhanced pulse sequences. R_1 spin-relaxation rates were measured with relaxation delays of 0.0020 (twice), 0.050, 0.12, 0.22 (twice), 0.36, 0.54, and 0.83 s. R_2 relaxation rates were obtained with total relaxation delays of 0 (twice), 0.017, 0.33, 0.051 (twice), 0.068, 0.085, and 0.12 s. The recycle delay in all R_1 and R_2 relaxation measurements was 2.5 s. The heteronuclear cross-relaxation rate was obtained from NOE experiments by interleaving pulse sequences with and without proton saturation. The recycle delay and proton-saturation time in hNOE measurements were 4.5 and 3.0 s, respectively. All relaxation spectra were acquired with a ^{15}N frequency of 118 ppm and a ^{1}H carrier set coincident with the water resonance; spectral widths were 9603 and 2595 Hz in the t_2 and t_1 dimensions, respectively, with 2048 and 256 complex points, respectively. hNOEs were determined from the ratio of peak heights for experiments with and without proton-saturation pulses. R_1 and R_2 rates were determined by fitting the peak heights using the program Curvefit, available from A. Palmer at Columbia University (New York, NY) (http://biochemistry.hs.columbia.edu/labs/palmer/software/curvefit.html).

Constant-time, relaxation-compensated Carr−Purcell−Meiboom−Gill (CPMG) experiments were performed under the following conditions. For samples containing 0.6 mM free PRL-3 and the complex with sodium orthovanadate, spectra were collected on the Bruker Avance 500 and 800 MHz spectrometer. Relaxation dispersion spectra were collected as a series of 17 two-dimensional data sets with CPMG field

Table 1. Statistics for 20 Vanadate-Bound PRL-3 Structures

no. of NOE restraints	2216
intraresidue and sequential ($\|i - j\| \leq 1$)	1079
medium-range ($1 < \|i - j\| < 5$)	564
long-range ($\|i - j\| \geq 5$)	573
dihedral angle restraints	209
hydrogen bond restraints	69
orientational restraints	119
coordinate precision (residues 9−158)	
backbone (Å)	0.93 ± 0.17
heavy atoms (Å)	1.35 ± 0.17
Ramachandran analysis	
most favored (%)	72.4
additionally allowed (%)	21.9
generously allowed (%)	3.5
disallowed (%)	2.2

strengths (υ_{cp}) of 50, 75, 100, 125, 150, 200 (twice), 250, 300, 400, 500 (twice), 600, 700, 800, 900, and 1000 Hz, and as reference spectra obtained by omitting the CPMG intervals in the pulse sequence. Each two-dimensional spectrum was recorded as a complex data matrix comprising 192 × 2048 points. Sixteen scans and/or free induction decays were recorded using a constant time delay of 40 ms and a recycle delay of 2.0 s. The intensities of cross-peaks were then converted into decay rates, R_2^{eff}, for a given υ_{cp}.[46] CPMG dispersion profiles were fit to a two-state exchange model using CATIA from F. Hansen (http://pound.med.utoronto.ca/~flemming/catia).

Structure Calculation of Vanadate-Bound PRL-3. For the structure calculation of vanadate-bound PRL-3, all NOE cross-peaks were assigned using combined automated and manual methods in CYANA 2.1. In total, 2216 meaningful NOE upper distance restraints were obtained. Backbone torsion angle restraints for 209 were derived from TALOS; 69 hydrogen bond restraints from the backbone amides were added as distance restraints, and 119 orientational restraints from ^{15}N RDC data were also included. Analyses of Ramachandran plots for the 20 lowest-energy structures were conducted using PROCHECK. Final coordinates and NOE constraints of vanadate-bound PRL-3 have been deposited in the Protein Data Bank (PDB) as entry 2MBC.

Model-Free Analysis. ^{15}N NMR relaxation parameters were analyzed in terms of internal motions of amide N−H bond vectors in the presence of overall anisotropic diffusion of the proteins. Protein amide backbone dynamics were characterized by fitting NMR spin-relaxation rates to one of five semiempirical forms of the spectral density function using a model-free formalism.[47,48]

The five models used to describe the spin-relaxation data are described according to their corresponding free parameters:[49] S^2 only for model 1, S^2 and τ_e for model 2, S^2 and R_{ex} for model 3, model 2 with R_{ex} for model 4, and S_f^2, S^2, and τ_e for model 5 (where τ_e is the internal correlation time, S^2 is the generalized order parameter, S_f^2 is the order parameter for fast motion with a typical correlation time of <10 ps, and R_{ex} is the additional line broadening due to assumed, two-site conformational exchange and depends on the equilibrium site populations, chemical shift differences, and rate of exchange between conformers). Motional parameters were fit to spin-relaxation data using the selection method described for FAST-Model-free[41] interfaced with Modelfree 4.01.[50,51] Model selection was based on the statistical testing protocol described previously by Mandel et al.[50] Pdbinertia and R2R1 Diffusion were downloaded from the homepage of Palmer's group (http://biochemistry.hs.columbia.edu/labs/palmer/software/diffusion.html) for calculating the inertia tensors from PDB coordinates of free PRL-3 (PDB entry 1V3A)[35] and our vanadate-bound PRL-3 and diffusion tensors from ^{15}N R_2/R_1 experimental relaxation data. The criteria for inclusion of residues in the diffusion tensor estimate relied on the method of Tjandra et al.[52] During the model-free analysis, an axially symmetric rotational diffusion tensor was used, the N−H bond lengths were assumed to be 1.02 Å, and the ^{15}N chemical shift anisotropy was assumed to be 160 ppm.[53,54] For each model, 300 randomly distributed data sets were generated. Models were selected by comparing the sum-square error of the optimal fit with a critical value of the distribution of 0.05. In cases where F statistics were applicable, comparisons were made with a critical value of the distribution of 0.20.

RESULTS AND DISCUSSION

Structure Calculation of Vanadate-Bound PRL-3. To date, two NMR solution structures calculated independently by Kim et al.[35] and Kozlov et al.[36] have been reported for PRL-3. Kim et al. calculated the structure of free PRL-3 in HEPES buffer, and Kozlov et al. calculated the structure of phosphate-bound PRL-3 in phosphate buffer. Comparison of the two structures revealed similar structures for secondary moieties but large differences for loop structures. The reason for these differences is the high flexibility of the loops in the free state, which resulted in a failure to detect the backbone amide signals from H103 to A111 and some of the terminal residues of free PRL-3 in the ^{1}H−^{15}N HSQC spectrum. Upon addition of phosphate ions to PRL-3 (phosphate-bound PRL-3), missing signals from the active-site loop regions from H103 to R110 appeared and gradually shifted in one direction until saturation was reached, indicating that the rate of exchange of phosphate ion between the free and bound states is faster than the NMR time scale.[35] In ^{1}H−^{15}N HSQC titration experiments, Kim et al. suggested that vanadate ions bind to PRL-3 in a slow−tight binding pattern, while phosphate ions bind in a fast−weak binding pattern.[35]

Because vanadate ions bind more tightly to PRL-3, the binding of vanadate ions may further stabilize the structure of these active-site loop regions of PRL-3, resulting in a closed conformation.[35] To determine the structure of vanadate-bound

dx.doi.org/10.1021/bi5003844 | Biochemistry 2014, 53, 4814−4825

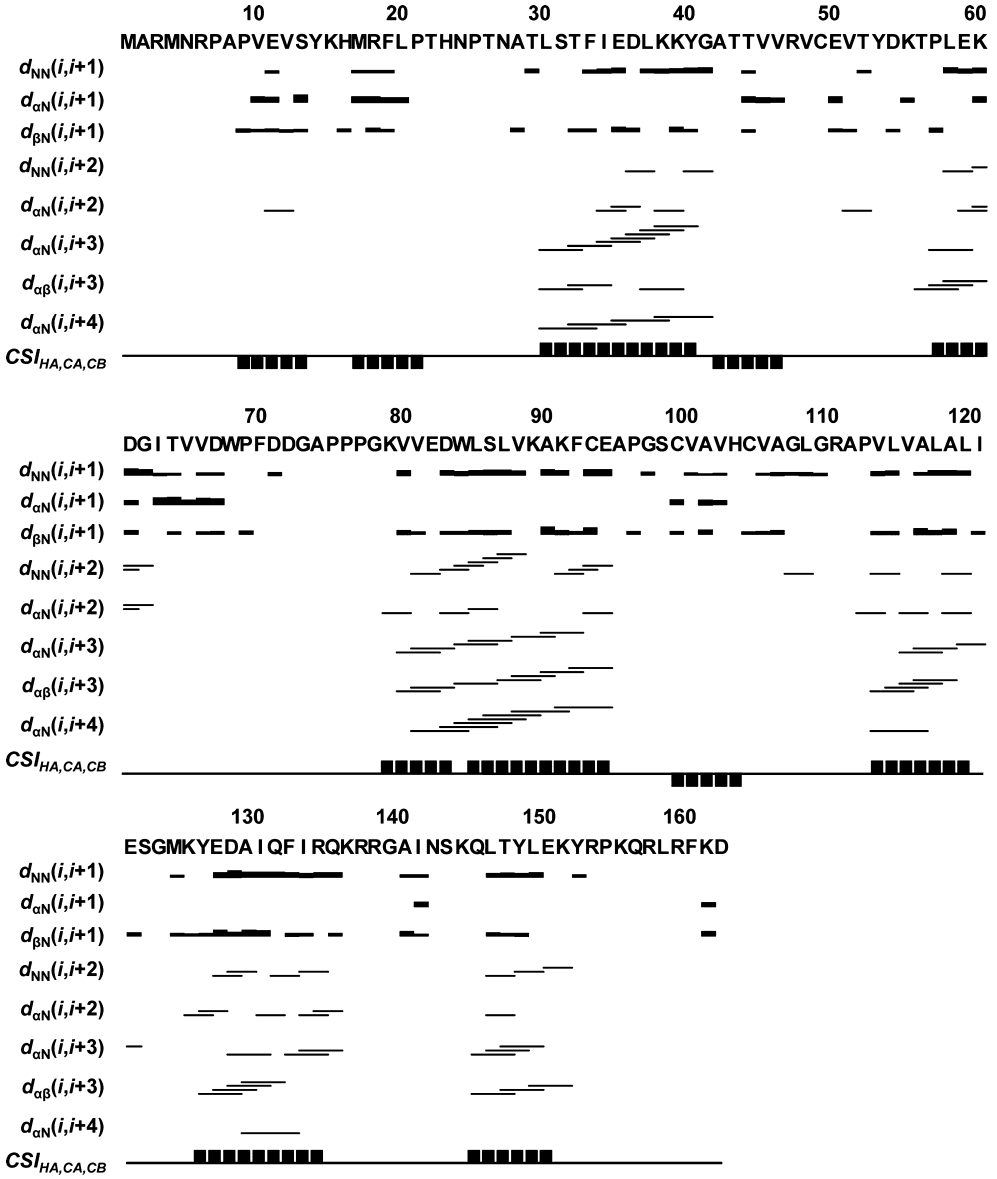

Figure 1. Sequence plot showing characteristic upper distance restraints along the vanadate-bound PRL-3 sequence derived from NOEs. Chemical shift indexes (CSIs) are shown below the sequence plot.

PRL-3, we assigned NMR resonances using ^{13}C- and ^{15}N-labeled PRL-3 (amino acids 1−162) and conventional heteronuclear methods. Tertiary structures were calculated using the CYANA software package[43] based on a total of 2216 NOE-derived distance restraints, 209 backbone torsion angle restraints, and 119 orientational restraints (Table 1). The sequence plots displaying characteristic upper distance restraints derived from NOEs and the chemical shift index of vanadate-bound PRL-3 are shown in Figure 1. The statistics for the structures are summarized in Table 1.

Figure 2A shows the backbone ^{1}H and ^{15}N chemical shift variations upon the addition of vanadate ion. Because local structural rearrangements occur when a ligand binds to a protein, these chemical shift variations were analyzed by comparing the $^{15}N-^{1}H$ HSQC spectra of free and vanadate-bound PRL-3s. As shown in Figure 2A, residues showing large chemical shift perturbations and signals that appear upon vanadate binding are indicated by green bars. In Figure 2B, the spatial location of chemical shift perturbation is indicated by a larger ribbon diameter; signals that appear upon vanadate binding are colored green. These residues are located mainly near active-site loop regions: on the $\alpha2-\beta4$ loop, WPD loop, P-loop, and $\alpha5-\alpha6$ loop.

The three-dimensional structure of our vanadate-bound PRL-3 is shown in Figure 2C, and that of free PRL-3 is shown in Figure 2D.[35,36] A best-fit superposition of the 20 lowest-energy conformers is also shown in Figure 3A. The root-mean-square deviation (rmsd) was 0.93 ± 0.17 Å for backbone atoms (N, C_α, and C′) and 1.35 ± 0.17 Å for all heavy atoms (non-hydrogen) of residues 9−158. The overall structures of free and vanadate-bound PRL-3s were very similar, except for the WPD loop, which exhibited large structural differences. The backbone rmsd of free and vanadate-bound forms was 2.70 Å, and that of phosphate-bound and vanadate-bound forms was 3.10 Å. In PRL-3s, the rmsd values of WPD loops (8.10 Å for free and vanadate-bound forms and 7.70 Å for phosphate-bound and vanadate-bound forms) were significantly larger than those of P-loops (3.70 Å for free and vanadate-bound

dx.doi.org/10.1021/bi5003844 | *Biochemistry* 2014, 53, 4814−4825

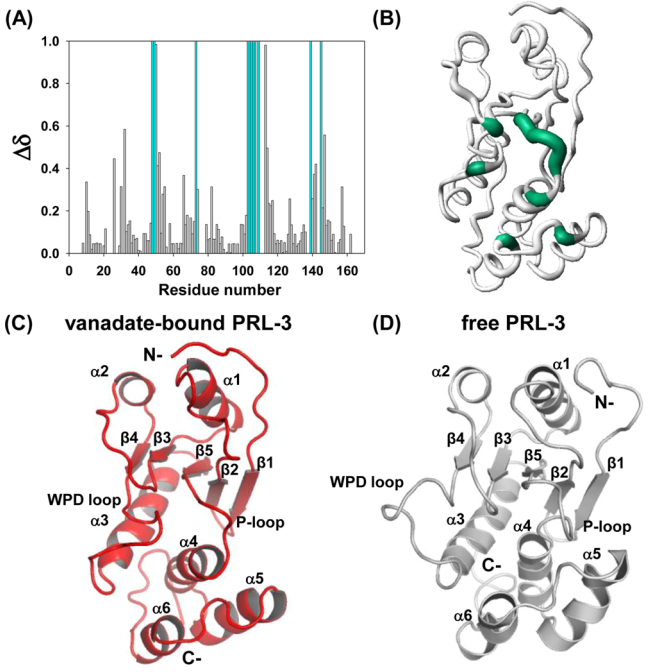

Figure 2. (A) Chemical shift perturbation and signals that appeared upon addition of the vanadate ion. Weighted average of the ^{15}N and ^{1}H chemical shift perturbations $\{\Delta\delta = [\delta H^2 + 0.2(\delta N^2)]^{1/2}\}$ of PRL-3 upon formation of a complex with a vanadate ion.[78] New signals that appeared upon vanadate binding are colored green, scaled to 1.0, and denoted by the green bars. (B) Spatial locations of chemical shift perturbations in a tubular drawing of vanadate-bound PRL-3 are shown by a larger ribbon diameter, and newly apparent signals are colored green with larger ribbon diameters. (C and D) Three-dimensional structures of vanadate-bound PRL-3 and free PRL-3 (PDB entry 1V3A), respectively.

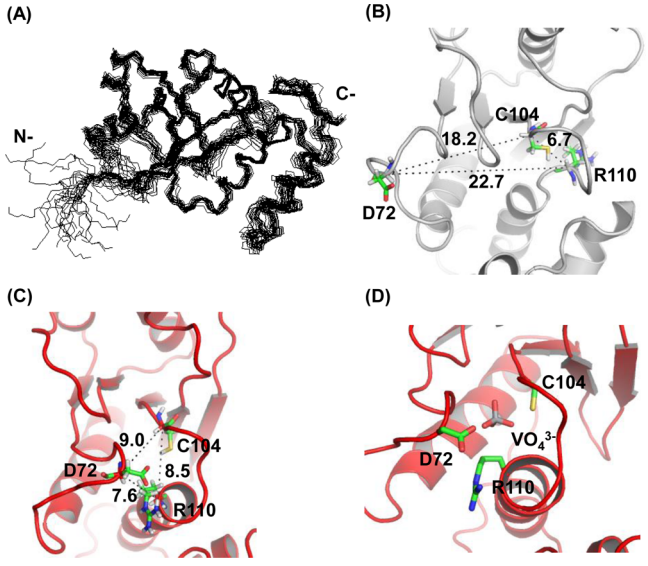

Figure 3. (A) Superimposition of the 20 backbone structures with the lowest-energy structure. (B and C) Comparison of three catalytic residues (D72, C104, and R110) in the active sites of free PRL-3 and vanadate-bound PRL-3, respectively. The C_α distances for each residue were measured; they are expressed in angstroms. (D) Active site of PRL-3 showing the vanadate position.

forms and 4.30 Å for phosphate-bound and vanadate-bound forms). The WPD loop of free PRL-3 extended beyond the active site, forming an open conformation, but those of PRL-3 complex forms were directed into the active site by the large movement, resulting in a closed conformation. Other distinct features were apparent at regions from helix $\alpha4$ to $\alpha6$ and the $\alpha5-\alpha6$ loop. Vanadate-bound PRL-3 had a longer $\alpha4$ helix in the G109–A111 region than free PRL-3, which may be expected because of the large movement and stabilization of the catalytic R110 residue to coordinate with vanadate in the active site. This conformational change in the $\alpha4$ region and P-loop also rearranged $\alpha5$ and $\alpha6$ helices and the $\alpha5-\alpha6$ loop, which moved slightly outside the bundles.

The topology of vanadate-bound PRL-3 resembled that of catalytic domains of dual-specificity phosphatases. The sequence of PRL-3 is highly similar to that of PRL-1 (79%), and PRLs are, in general, more homologous to dual-specificity phosphatases (Dusp23, 21%[55]) than to other tyrosine-specific PTPs. The catalytic residues in the WPD loop and P-loop are highly conserved in PRLs and dual-specificity phosphatases, whereas polybasic and prenylation motifs are conserved in PRLs. D72, C104, and R110 in PRL-3 should be close together to support the enzymatic reaction; thus, a substantial conformational rearrangement of PRL-3 may occur during binding of the substrate molecule. In the P-loop, C104 is the enzymatic nucleophile and R110 coordinates with the phosphate group on phosphotyrosine. D72 is believed to serve as a general acid.[56] Distances between the C_α atoms of these aspartic acid, cysteine, and arginine residues in the free form and those in the vanadate-bound form are compared in panels B and C of Figure 3. The WPD loop of free PRL-3 was found to be in a widely open conformation (Figure 3B); thus, the D72 residue was distant from the phosphate-binding loop, 18.2 Å from C104 and 22.7 Å from R110. In contrast, the WPD loop of vanadate-bound PRL-3 was pulled toward the phosphate-binding loop (Figure 3C). The important NOE constraints that cause the WPD loop to have a closed conformation originate from the proximity among C49–F70, C49–D71, E50–D71, and F70–L114. These conformations were further refined by incorporating RDCs as additional structural restraints. We also docked the vanadate ion into the active site and proposed the binding model based on the chemical shift perturbation as shown in panels A and B of Figure 2. In Figure 3D, the vanadate ion is bound to the center of active-site loops, and this binding model is very similar to that of sulfate-bound PRL-1.[57] The closed conformation of the WPD loop is stabilized by the electrostatic interactions between negatively charged oxygen atoms of the vanadate ion and amide backbones in the active-site loops.

PRLs belong to a novel class of PTPs containing a C-terminal prenylation motif. The prenylation motif is important for membrane association, intracellular localization, and trimerization in the cell. Although the prenylation motif of PRL-1 is truncated, the polybasic region in the C-terminus is also required for plasma membrane association.[36] In the case of PRL-1, replacement of all six positively charged residues in the polybasic stretch with alanine residues yielded a mutant that failed to localize to the membrane, suggesting that prenylation alone in PRL-1 is insufficient for plasma membrane localization and that the C-terminal polybasic region is required for proper membrane targeting of PRL-1.[57,58]

The polybasic regions of free PRL-3[35] and vanadate-bound PRL-3 (this study) are compared in Figure 4. Polybasic regions of the free form (Figure 4A) are close and almost parallel to the $\alpha3$ helix. However, the distal part of the polybasic region of

dx.doi.org/10.1021/bi5003844 | Biochemistry 2014, 53, 4814–4825

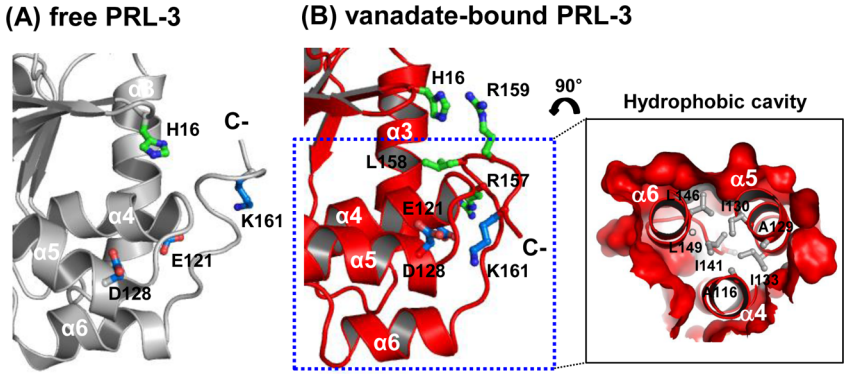

Figure 4. Comparison of the polybasic regions in (A) free PRL-3 (PDB entry 1V3A) and (B) vanadate-bound PRL-3. The hydrophobic cavity formed by helices α4–α6 of the vanadate-bound form (blue dotted box) is rotated 90° and magnified in the right panel. The hydrophobic residues in this cavity are depicted as gray sticks. H16, R157, L158, and R159 are depicted as green sticks and E121, D128, and K161 that contribute to the unique conformation of the polybasic region by electrostatic interactions as blue sticks.

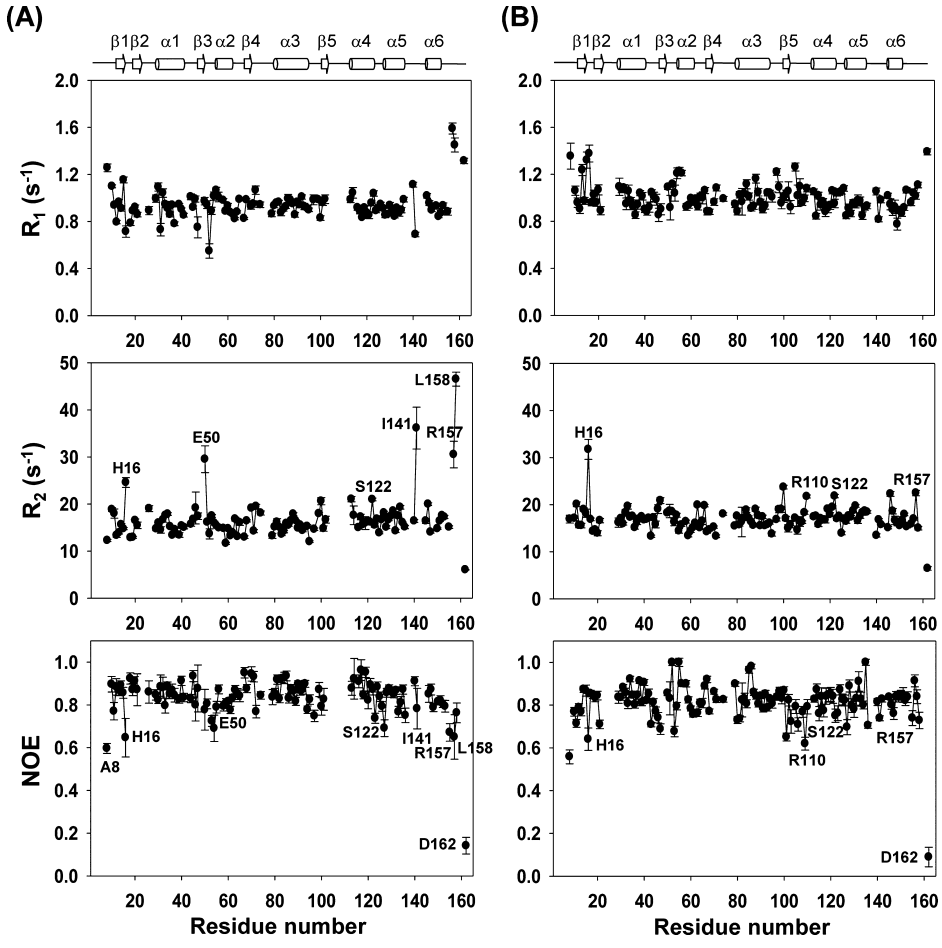

Figure 5. Summary of NMR spin-relaxation results. NMR data are displayed as a function of residue number for (A) free PRL-3 and (B) vanadate-bound PRL-3. Breaks in lines indicate regions of missing data resulting from a missing peak, the presence of a proline residue, data peak overlap, or an inadequate signal-to-noise ratio. The secondary structures are shown above the plots.

vanadate-bound form is bent, and as a result, R157, L158, and R159 form a loop structure, as shown in Figure 4B. H16 makes close contact with these residues (green stick in Figure 4B), and the polybasic region of vanadate-bound PRL-3 at the C-terminus faces helices α5 and α6, even though they are part of the C-terminal region, which can be, in general, very flexible. We also suggest that electrostatic interactions between the positively charged residue K161 in the polybasic region and negatively charged residue E121 or D128 (blue sticks in Figure 4B) contribute to this unique conformation of the C-terminal region. This distinctive structure of vanadate-bound PRL-3 is derived from long-range distance constraints among L117–Y152, I120–P154, E121–R157, K89–R157, L85–R157, A118–L158, L85–L158, S86–L158, V88–L158, K89–L158, E121–L158, S122–L158, G123–L158, and K125–D162.

dx.doi.org/10.1021/bi5003844 | *Biochemistry* 2014, 53, 4814–4825

Protein prenylation involves the transfer of either a farnesyl (C15) or geranyl (C20) moiety to a C-terminal cysteine residue.[59] It has been reported that PRL-3 is farnesylated and associated with the cell surface membrane.[60] Our vanadate-bound PRL-3 structure showed that the hydrophobic cavity formed by helices α4−α6 is approximately 14−15 Å deep and, thus, can hold a farnesyl chain with a length of approximately 12−13 Å. The prenylation motif from R169 to M173 was truncated in this study to produce a soluble protein. The farnesylated moiety of PRL-3, attached to the end of the prenylation motif of PRL-3, may be inserted into the hydrophobic lipid-binding pocket formed by residues P112, V113, A116, I120, Y126, A129, I130, I133, A140, I141, L146, and L149, as shown in Figure 4B (right panel). The conformation of the polybasic region located near this hydrophobic cavity in our vanadate-bound PRL-3 may favor holding the prenylated chain.

NMR Relaxation Study. R_1 and R_2 values are sensitive to different motional frequencies. R_1 values provide information regarding motional properties with a frequency of approximately 10^8−10^{12} s^{-1}, whereas R_2 values, in addition to depending on motion occurring at these frequencies, are also sensitive to dynamics on a microsecond-to-millisecond time scale. Hence, via measurement of both R_1 and R_2, it is possible to obtain dynamic information over a large motional regime.[61] Only ^{15}N T_1 and T_2 values for residues from A90 to I120 of free and vanadate-bound forms were reported by Kim et al.[35] Here, we measured R_1, R_2, and hNOE values for all backbone amide ^{15}N signals of complete free and vanadate-bound PRL-3s. ^{15}N NMR relaxation data for free and vanadate-bound PRL-3s are shown in Figure 5. The average R_1, R_2, and hNOE values for free PRL-3 were 0.94 ± 0.02 s^{-1}, 16.61 ± 0.56 s^{-1}, and 0.82 ± 0.07, respectively, and the corresponding values for vanadate-bound PRL-3 were 0.99 ± 0.05 s^{-1}, 16.80 ± 0.45 s^{-1}, and 0.84 ± 0.05, respectively.

NMR spin-relaxation rate data for free PRL-3 revealed unexpectedly large R_2 values (>20 s^{-1}) for the backbone N-H groups of H16 (R_2 = 24.58 s^{-1}), E50 (R_2 = 29.53 s^{-1}), V100 (R_2 = 20.61 s^{-1}), V113 (R_2 = 21.04 s^{-1}), S122 (R_2 = 20.98 s^{-1}), I141 (R_2 = 36.14 s^{-1}), R157 (R_2 = 30.52 s^{-1}), and L158 (R_2 = 46.52 s^{-1}), as shown in Figure 5A. These large R_2 values could result from the conformational exchange (R_{ex}) of the protein on a microsecond-to-millisecond time scale. E50 is located in the highly conserved CX_nE motif (where X is any amino acid and n is the number of amino acids between the C and E residues) in both PRLs and PTPs. This motif is known to play an important role in the general catalytic mechanism or stabilization of the catalytic pocket of dual-specificity phosphatases.[22] Upon binding to vanadate, residue I141, which appears to be solvent-exposed in free PRL-3, is buried in the hydrophobic lipid-binding pocket in vanadate-bound PRL-3 (Figure 6), exhibiting a large decrease in R_2 (from 36.14 to 16.79 s^{-1}). Because NMR signals from residues in the WPD loop as well as P-loop region appeared only in vanadate-bound PRL-3, we found that conformational exchanges of R110 at the catalytic site are closely related to the loop closure upon binding of vanadate ions. S122 and R157 also showed a conformational exchange in vanadate-bound PRL-3. R157 and L158 are located in the polybasic region of PRL-3 and are in close contact with S122 in helix α4 (Figure 6). Although the prenylation motif (from R169 to M173) of PRL-3 was truncated in this study, the structure and spin-relaxation data imply that the polybasic region is in close contact with helices α3 and α4. H16, which is

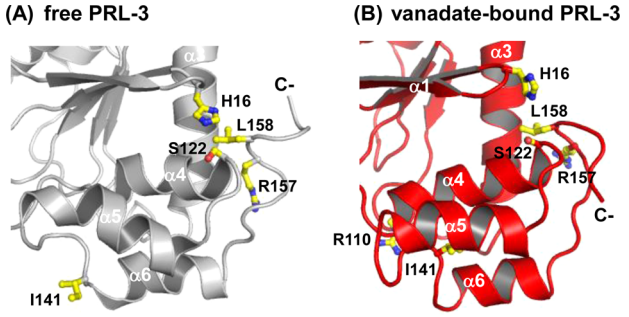

Figure 6. NMR-detected slow motions in (A) free PRL-3 and (B) vanadate-bound PRL-3. The residues exhibiting large R_2 values (>20 s^{-1}) are depicted as yellow sticks.

located on the opposite end of the active site, is close to the polybasic region (Figure 6), and it is likely that the high R_2 value of H16 (24.6 s^{-1} in the free form and 31.7 s^{-1} in the vanadate-bound form) might also be related to the function of the polybasic region. The rates of conformational exchange of R157 (30.52 to 22.48 s^{-1}) and L158 (46.52 to 15.02 s^{-1}) were decreased in vanadate-bound PRL-3, suggesting that binding of vanadate to PRL-3 induces conformational changes and the flexibility of the C-terminal region. Notably, R157 and L158 are closer to helices α3 and α4 in the vanadate-bound form than in the free form (Figure 6). Therefore, these structural changes in vanadate-bound PRL-3 may result from stronger interactions with residues in helices α3 and α4.

To investigate motions in PRL-3 on the microsecond-to-millisecond time scale, we performed CPMG experiments with free and vanadate-bound PRL-3s; the experimentally fitted data at 800 MHz NMR are shown in Figure 7. Differences in R_2^{eff} values are plotted as a function of amino acid sequence because a chemical exchange at the protein backbone was evident from these differences measured at long (ν_{cp} = 50 Hz) and short (ν_{cp} = 1000 Hz) interpulse delays. Residues H16, E50, R110, I141, R157, and L158, which showed high R_2 values in free and vanadate-bound PRL-3s, were identified as residues that undergo chemical exchange on a microsecond-to-millisecond time scale. Loria et al. determined exchange rates (k_{ex}) between open and closed states for the WPD loop of PTP1B by NMR relaxation dispersion studies.[40] A k_{ex} value of 367 s^{-1} was calculated for residues W68, F70, and A74 in the WPD loop, having a major population of open conformers, P_{open}, of ∼98%. However, a k_{ex} value of 423 s^{-1} was calculated for residues in the polybasic region (R157 and L158), having a major population of open conformers, P_{open}, of ∼97% (Table 2). From these data, we also obtained a k_{close} of 7 s^{-1} and a k_{open} of 360 s^{-1} for the WPD loop, which were 2.5−3-fold slower than those of PTP1B (k_{close} = 22 s^{-1}, and k_{open} = 890 s^{-1}),[40] suggesting that the WPD loop motion of PRL-3 is slower than that of PTP1B. As shown in Table 2, the polybasic region in free PRL-3 closes (k_{close} = 14 s^{-1}) with a rate constant very similar to that of the WPD loop, implying that this motion in the polybasic region may be closely related to prenylation and membrane association.

The hNOE data of backbone ^{15}N nuclei are sensitive to motion on a nanosecond-to-picosecond time scale. hNOE is typically most sensitive to the high-frequency motion of the backbone, with values near 1.0 indicating a lack of such motion and lower values indicating increased local flexibility of the polypeptide.[62,63] The average hNOE values of free and vanadate-bound PRL-3s were similar (0.82 and 0.84,

dx.doi.org/10.1021/bi5003844 | Biochemistry 2014, 53, 4814−4825

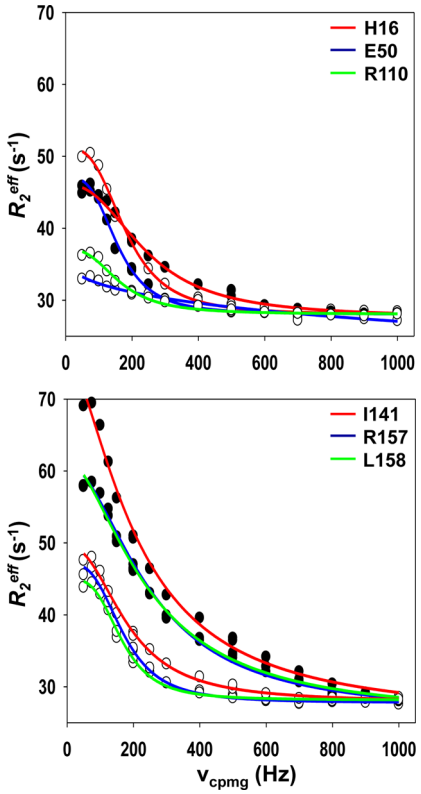

Figure 7. Chemical exchanges in free and vanadate-bound PRL-3s. CPMG dispersion curves for the free form (filled circles) and the vanadate-bound form (empty circles). Values of R_2^{eff} are plotted vs ν_{cp} for H16, E50, R110, I141, R157, and L158 recorded using an 800 MHz NMR spectrometer. Solid lines indicate fitted curves.

Table 2. Summary of Motions in Free PRL-3

region	k_{ex} (s^{-1})	k_{close} (s^{-1})	k_{open} (s^{-1})	P_{open} (%)	P_{close} (%)
WPD loop (W68, F70, A74)	367 ± 9	7 ± 0.3	360 ± 9	98	2
polybasic region (R157, L158)	423 ± 10	12 ± 0.4	411 ± 10	97	3

respectively). However, if the paucity of residues that show resonance in free PRL-3 because of the structural flexibility and the resulting low hNOE values is taken into account, the protein appeared to adopt a somewhat more rigid structure upon binding of vanadate. This finding suggests that vanadate binding may contribute to stabilization of the protein by inducing conformational reorganization. Interestingly, the average hNOE value of the C-terminal polybasic region increased from 0.64 to 0.74 upon binding of vanadate ions. Therefore, the rigidity of the polybasic region increased upon ligand binding.

^{15}N NMR relaxation measurements can be analyzed by a model-free formalism[49] to obtain information regarding global and site-specific dynamics. Using an axially symmetric diffusion tensor, we found that the rotational correlation time, τ_m, was 9.76 ± 0.44 and 9.80 ± 0.31 ns in free and vanadate-bound PRL-3, respectively, with D_{par}/D_{per} values of 1.25 and 1.21 ns, respectively. These values are in agreement with theoretical predictions based on the molecular mass of PRL-3 and hydrodynamic calculations.[64] Backbone motional parameters for free and vanadate-bound PRL-3s obtained by model-free analysis are shown in Figure 8. In total, five residues displayed an R_{ex} of >10 in both free and vanadate-bound forms, most of which were located in the loop region. Only L158, which showed a large R_2 value, was not described by any model in either free or vanadate-bound PRL-3.

Although NMR signals of the P-loop of free PRL-3 were not detected because of the high flexibility, signals of these residues could be detected in vanadate-bound PRL-3, which implies that these residues adopt a less flexible structure in the vanadate-bound form. This is consistent with the protein-tyrosine phosphatases SHP-1[65] and PTP1B,[34] in which the flexibility of the P-loop is related to the activity of the catalytic domain of PTP, as suggested by sequence alignment and structural analyses.[63] Internal motion on a nanosecond-to-picosecond time scale results in generalized order parameter (S^2) values that are less than unity. As shown in Figure 8, free PRL-3 exhibited high S^2 values, except in regions such as the P-loop. The average S^2 value for the entire protein was 0.93 ± 0.02 and 0.96 ± 0.02 for free and vanadate-bound PRL-3s, respectively, indicating a well-ordered backbone structure with restricted internal motion on a nanosecond-to-picosecond time scale. The average S^2 value increased slightly upon vanadate binding. Considering the flexibility of the P-loop, the average S^2 value would be expected to further increase upon vanadate binding. Thus, binding of vanadate appears to render the PRL-3 molecule more rigid by decreasing its overall level of internal motion. Upon formation of the complex with vanadate, a large increase (≥0.05) in average S^2 values occurred for active-site loops $\beta3-\alpha2$ and $\alpha5-\alpha6$. The S^2 values of the following residues decreased below a threshold of 0.75: A8, H16, E50, R157, and D162 in the free form and D162 in the vanadate-bound form. All of these residues were located in loop or terminal regions. The S^2 values are indicated in color on the ribbon structures of free and vanadate-bound PRL-3 in panels A and B of Figure 9, respectively, and the R_{ex} values for the residues are shown with a larger ribbon diameter. As shown in Figure 9, binding of a vanadate ion to PRL-3 increased the overall rigidity of PRL-3, including that of its P-loop. R157 in the polybasic region is in close contact with S122 in helix $\alpha4$ in the vanadate-bound form, and S122 and R157 showed conformational exchange in vanadate-bound PRL-3 (Figure 6). Moreover, H16, which is in close contact with the polybasic region, showed a large conformational exchange in both forms. Because R110 is known to coordinate with the phosphate group on phosphotyrosine, this residue may undergo conformational exchange between the major closed formation and the minor open conformation by coordinating with a vanadate ion in vanadate-bound PRL-3.

CONCLUSION

Recent interest in PRLs stems from their roles in regulating cell proliferation and promoting cell migration, invasion, and metastasis. With regard to PRL-3, it is believed that substantial conformational rearrangement may occur during binding of the substrate molecule.[35,36] In the study presented here, we determined the three-dimensional structure of vanadate-bound PRL-3 in HEPES buffer. Vanadate binding in PRL-3 induces WPD loop closure to achieve a fully active conformation. Comparisons of free and vanadate-bound forms showed large differences in the structure of the WPD loop. D72, C104, and R110, which participate in the enzymatic reaction, were close together only in our vanadate-bound PRL-3. This closed conformation resulted in close contact between the WPD loop (F70 and D71) and the $\beta3-\beta4$ loop (C49 and

dx.doi.org/10.1021/bi5003844 | Biochemistry 2014, 53, 4814−4825

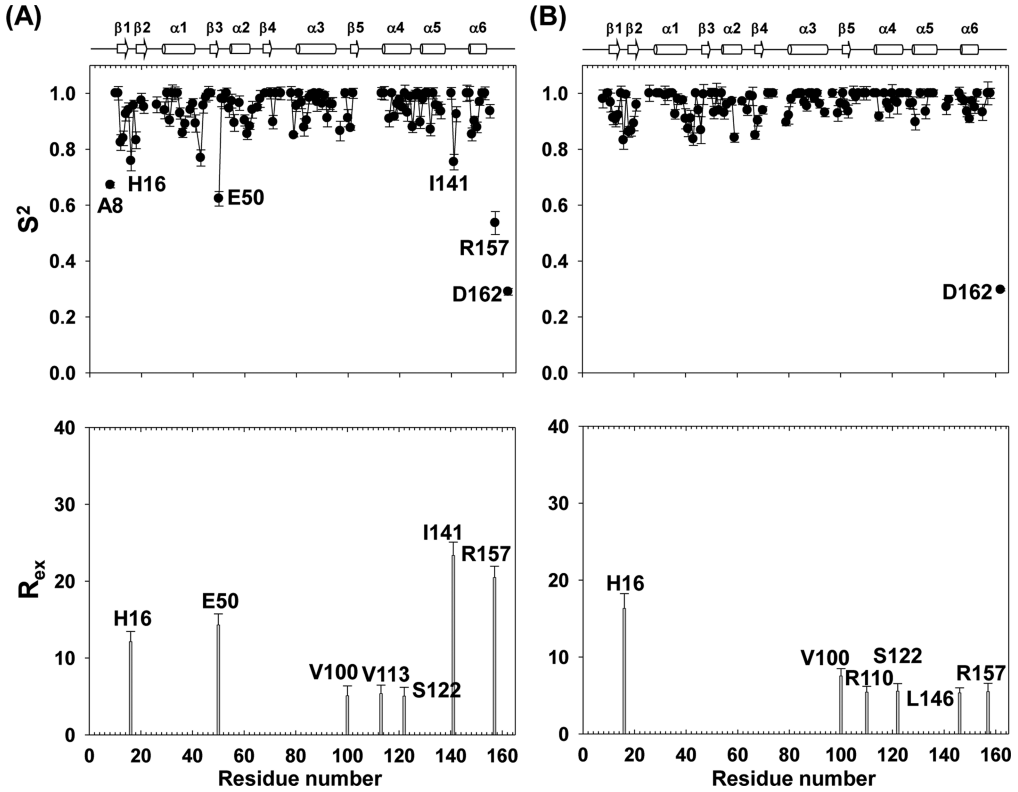

Figure 8. Results of the model-free analysis of (A) free PRL-3 and (B) vanadate-bound PRL-3. Breaks in lines indicate regions of missing data resulting from the presence of a proline residue, data peak overlap, an inadequate signal-to-noise ratio, or residues for which no motional model could be fitted. The secondary structures are shown above the plots.

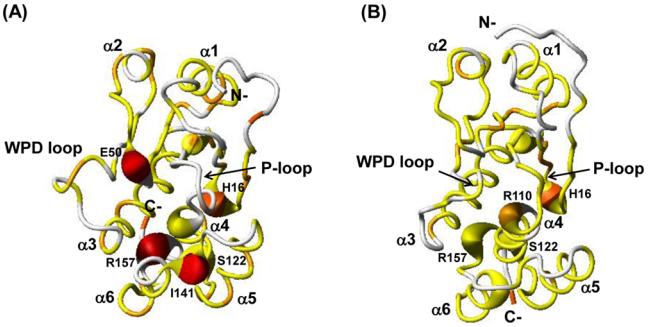

Figure 9. Spatial location of NMR-derived dynamic parameters. Values of the order parameter, S^2, are color-coded onto tubular drawings of (A) free PRL-3 and (B) vanadate-bound PRL-3. The color scheme is as follows: red for $S^2 < 0.8$, orange for $0.8 \leq S^2 < 0.9$, and yellow for $S^2 \geq 0.9$. Residues with R_{ex} values of ≥5.0 are shown with a larger ribbon diameter. White indicates proline, unassigned residues, and residues that are not fit in model-free analysis. This figure was prepared using MolMol.[79]

E50) as well as helix α4 (L114). Helices α4−α6 and the α5−α6 loop of vanadate-bound PRL-3 also showed large differences compared to those in the free PRL-3 structure because of the conformational rearrangement of the α4 region and P-loop. According to these conformational changes, helices α4 and α6 and the α5−α6 loop also moved slightly outside, which may have induced the structural rearrangement of the C-terminal polybasic region in vanadate-bound PRL-3. When we compared interface regions between helices α4−α6 and the C-terminal polybasic region in free and vanadate-bound PRL-3, the negatively charged residues E121 and D128 in helices α5 and α6 were much closer to the positively charged K161 residue in the polybasic region of the vanadate-bound form than in that of the free form (Figure 4). Therefore, we suggest that vanadate binding induced structural changes in the WPD loop, P-loop, helices α4−α6, and the polybasic region.

The X-ray structure of a prenylated Ypt1·GDI complex revealed that the prenylated moiety is located on the hydrophobic surface of the protein containing hydrophobic residues V127, P128, A129, A134, L139, M140, M148, L152, I155, F192, I193, M197, W200, Y205, and L218 between helices D and E.[66] PRLs have been demonstrated to be the only phosphatases of the PTP superfamily that carry the CAAX motif and that are farnesylated *in vivo*.[22,67−71] A recent molecular docking study also suggested that the lipid chains may be able to reach the hydrophobic stretches consisting of aliphatic residues in helices α4−α6.[22] In addition, PRLs are farnesylated and geranylated, whereas PRL-3 is only farnesylated.[67] In this study, we proposed that the farnesyl chain may be inserted into the hydrophobic cavity formed by helices α4−α6 of vanadate-bound PRL-3 (Figure 4B). Hydrophobic residues in helices α4−α6 and α5−α6 loop regions, e.g., I141, are buried deeply in the hydrophobic pocket formed by helices α4−α6 of vanadate-bound PRL-3, which may allow interactions with the lipid chain at the prenylation motif while I141 in free PRL-3 is exposed to the outside. The depth of this hydrophobic cavity (~14−15 Å), shown in Figure 4B, is not sufficient to accommodate the longer geranyl chain (~17−18 Å) but is sufficient to hold a farnesyl chain (~12−13 Å). However, PRL-1 (PDB entry 1ZCK) has longer α4 and α6 helices than PRL-3; thus, the hydrophobic pocket of PRL-1, with a depth of approximately 18−19 Å, is sufficiently deep to accommodate both farnesyl and geranylgeranyl chains (data not shown).

dx.doi.org/10.1021/bi5003844 | *Biochemistry* 2014, 53, 4814−4825

These results indicate that PRL-3 prefers the shorter farnesyl chain to the geranylgeranyl chain at its prenylation site.

^{15}N relaxation measurements allowed us to study the internal motion of the ligand-binding epitope of PRL-3. These motions are identified by the R_{ex} term, which indicates exchanges between conformations in various chemical environments.[63] Our data showed rigid backbone dynamics on a picosecond-to-nanosecond time scale for both free and vanadate-bound PRL-3s. However, new signals of residues near active sites, including those in the WPD loop and P-loop (Figure 2B, colored green), appeared in the ^{1}H−^{15}N HSQC spectra of vanadate-bound PRL-3, suggesting that these regions become more rigid upon vanadate binding.

Protein motion on a slow time scale, which has high R_2 values, can participate directly in ligand and/or protein recognition processes. Many biological processes on micro-second-to-millisecond time scales, including ligand binding, protein folding, and enzyme catalysis, can be characterized by relaxation dispersion techniques.[63,72−76] In this study, R_2 values of R110 were increased upon vanadate binding, implying that this slow motion is closely related to ligand binding. We also demonstrated for the first time that H16 protrudes toward the polybasic region and chemical exchanges of H16 in addition to R157 and L158, which form a loop at the C-terminal polybasic region, may be closely correlated with prenylation of PRL-3 (Figure 6). On the basis of the structure of vanadate-bound PRL-3, we also propose that the farnesyl chain at the truncated prenylation motif from R169 to M173 of PRL-3 may be inserted into the hydrophobic pockets formed by residues in helices α4−α6, including I141, which exhibits a large conformational exchange in the free form.

The WPD loop of PRL-3 must be closed for ligand binding; thus, the rate at which the loop is closed could potentially be related to enzymatic kinetics. Recently, Loria et al. calculated k_{close} values of WPD loops in human PTP1B and YopH using ^{15}N CPMG relaxation dispersion data.[40] In their study, the authors successfully obtained k_{close} values that were very similar to the experimental values, $k_{cleavage}$, of PTP1B and YopH.[40] The dynamics and conformational properties of loops containing proline residues are significantly slower than the dynamics and conformational properties of those containing other amino acids.[77] The closing rate of PRL-3 obtained here using CPMG relaxation data was 3-fold slower than that of human PTP1B because PRL-3 has more proline residues (P69, P75, P76, and P77) than PTP1B (P180, P185, and P188) in the WPD loop.[40] The slower motions likely reflect the physiological role of PRL-3 as a tight regulator of cellular processes, and different motions of these enzymes may allow the regulation of cellular processes by interacting with different substrates and binding partners.[40] Interestingly, the rate of WPD loop motion (k_{close} = 7 s^{-1}, and k_{open} = 367 s^{-1}) was very similar to that of the polybasic region (k_{close} = 12 s^{-1}, and k_{open} = 411 s^{-1}). Although the prenylation motif (from R169 to M173) of PRL-3 was truncated in this study, loop closing of the polybasic region may occur concomitantly with prenylation.

We found that conformational changes and the flexibility of the WPD loop and P-loop are important in ligand binding. The structural rearrangement that occurs when vanadate binds to the active site of PRL-3 results in a closed conformation, which is required for catalytic activity.

AUTHOR INFORMATION

Corresponding Author

*Department of Bioscience and Biotechnology, Konkuk University, Seoul 143-701, South Korea. Telephone: +822-450-3421. Fax: +822-447-5987. E-mail: ymkim@konkuk.ac.kr.

Funding

This work was supported by grants from the Priority Research Centers Program (2009-0093824) and the Basic Science Research Program (2013R1A1A2058021) through the National Research Foundation of Korea funded by the Ministry of Education, Science, and Technology, and by a grant from the High Field NMR Research Program of the Korea Basic Science Institute (to Y.K.). This work was also supported by Global Frontier Project NRF-M1AXA002-2010-0029765 (to Y.H.J.).

Notes

The authors declare no competing financial interest.

ABBREVIATIONS

CSI, chemical shift index; CPMG, Carr−Purcell−Meiboom−Gill; HEPES, 4-(2-hydroxyethyl)-1-piperazineethanesulfonic acid; HSQC, heteronuclear single-quantum coherence; NMR, nuclear magnetic resonance; NOE, nuclear Overhauser effect; NOESY, nuclear Overhauser effect spectroscopy; PRL, phosphatase of regenerating liver; pTyr, phosphotyrosine; PTP, protein tyrosine phosphatase; RDC, residual dipolar coupling; rmsd, root-mean-square deviation; TOCSY, total correlation spectroscopy.

REFERENCES

(1) Vintonyak, V. V., Antonchick, A. P., Rauh, D., and Waldmann, H. (2009) The therapeutic potential of phosphatase inhibitors. *Curr. Opin. Chem. Biol. 13*, 272−283.

(2) Hunter, T. (1998) The phosphorylation of proteins on tyrosine: Its role in cell growth and disease. *Philos. Trans. R. Soc., B B353*, 583−605.

(3) Pulido, R., and Hooft van Huijsduijnen, R. (2008) Protein tyrosine phosphatases: Dual-specificity phosphatases in health and disease. *FEBS J. 275*, 848−866.

(4) Matter, W. F., Estridge, T., Zhang, C., Belagaje, R., Stancato, L., Dixon, J., Johnson, B., Bloem, L., Pickard, T., Donaghue, M., Acton, S., Jeyaseelan, R., Kadambi, V., and Vlahos, C. J. (2001) Role of PRL-3, a human muscle-specific tyrosine phosphatase, in angiotensin-II signaling. *Biochem. Biophys. Res. Commun. 283*, 1061−1068.

(5) Mohn, K. L., Laz, T. M., Hsu, J. C., Melby, A. E., Bravo, R., and Taub, R. (1991) The immediate-early growth response in regenerating liver and insulin-stimulated H-35 cells: Comparison with serum-stimulated 3T3 cells and identification of 41 novel immediate-early genes. *Mol. Cell. Biol. 11*, 381−390.

(6) Diamond, R. H., Cressman, D. E., Laz, T. M., Abrams, C. S., and Taub, R. (1994) PRL-1, a unique nuclear protein tyrosine phosphatase, affects cell growth. *Mol. Cell. Biol. 14*, 3752−3762.

(7) Montagna, M., Serova, O., Sylla, B. S., Feunteun, J., and Lenoir, G. M. (1995) A 100-kb physical and transcriptional map around the EDH17B2 gene: Identification of three novel genes and a pseudogene of a human homologue of the rat PRL-1 tyrosine phosphatase. *Hum. Genet. 96*, 532−538.

(8) Cates, C. A., Michael, R. L., Stayrook, K. R., Harvey, K. A., Burke, Y. D., Randall, S. K., Crowell, P. L., and Crowell, D. N. (1996) Prenylation of oncogenic human PTP (CAAX) protein tyrosine phosphatases. *Cancer Lett. 110*, 49−55.

(9) Zeng, Q., Hong, W., and Tan, Y. H. (1998) Mouse PRL-2 and PRL-3, two potentially prenylated protein tyrosine phosphatases homologous to PRL-1. *Biochem. Biophys. Res. Commun. 244*, 421−427.

(10) Lin, M. D., Lee, H. T., Wang, S. C., Li, H. R., Hsien, H. L., Cheng, K. W., Chang, Y. D., Huang, M. L., Yu, J. K., and Chen, Y. H.

(2013) Expression of phosphatase of regenerating liver family genes during embryogenesis: An evolutionary developmental analysis among *Drosophila*, amphioxus, and zebrafish. *BMC Dev. Biol. 13* (18), 1−13.
(11) Navis, A. C., van den Eijnden, M., Schepens, J. T., Hooft van Huijsduijnen, R., Wesseling, P., and Hendriks, W. J. (2010) Protein tyrosine phosphatases in glioma biology. *Acta Neuropathol. 119*, 157−175.
(12) Saha, S., Bardelli, A., Buckhaults, P., Velculescu, V. E., Rago, C., St Croix, B., Romans, K. E., Choti, M. A., Lengauer, C., Kinzler, K. W., and Vogelstein, B. (2001) A phosphatase associated with metastasis. *Science 294*, 1343−1346.
(13) Al-Aidaroos, A. Q., and Zeng, Q. (2010) PRL-3 phosphatase and cancer metastasis. *J. Cell. Biochem. 111*, 1087−1098.
(14) Fiordalisi, J. J., Dewar, B. J., Graves, L. M., Madigan, J. P., and Cox, A. D. (2013) Src-mediated phosphorylation of the tyrosine phosphatase PRL-3 is required for PRL-3 promotion of Rho activation, motility and invasion. *PLoS One 8* (5), e64309.
(15) Forte, E., Orsatti, L., Talamo, F., Barbato, G., De Francesco, R., and Tomei, L. (2008) Ezrin is a specific and direct target of protein tyrosine phosphatase PRL-3. *Biochim. Biophys. Acta 1783*, 334−344.
(16) Orsatti, L., Forte, E., Tomei, L., Caterino, M., Pessi, A., and Talamo, F. (2009) 2-D difference in gel electrophoresis combined with Pro-Q diamond staining: A successful approach for the identification of kinase/phosphatase targets. *Electrophoresis 30*, 2469−2476.
(17) Mizuuchi, E., Semba, S., Kodama, Y., and Yokozaki, H. (2009) Down-modulation of keratin 8 phosphorylation levels by PRL-3 contributes to colorectal carcinoma progression. *Int. J. Cancer 124*, 1802−1810.
(18) Tian, W., Qu, L., Meng, L., Liu, C., Wu, J., and Shou, C. (2012) Phosphatase of regenerating liver-3 directly interacts with integrin β1 and regulates its phosphorylation at tyrosine 783. *BMC Biochem. 13* (22), 1−8.
(19) Zheng, P., Liu, Y. X., Chen, L., Liu, X. H., Xiao, Z. Q., Zhao, L., Li, G. Q., Zhou, J., Ding, Y. Q., and Li, J. M. (2010) Stathmin, a new target of PRL-3 identified by proteomic methods, plays a key role in progression and metastasis of colorectal cancer. *J. Proteome Res. 9*, 4897−4905.
(20) Semba, S., Mizuuchi, E., and Yokozaki, H. (2010) Requirement of phosphatase of regenerating liver-3 for the nucleolar localization of nucleolin during the progression of colorectal carcinoma. *Cancer Sci. 101*, 2254−2261.
(21) Lian, S., Meng, L., Liu, C., Xing, X., Song, Q., Dong, B., Han, Y., Yang, Y., Peng, L., Qu, L., and Shou, C. (2013) PRL-3 activates NF-κB signaling pathway by interacting with RAP 1. *Biochem. Biophys. Res. Commun. 430* (1), 196−201.
(22) Rios, P., Li, X., and Köhn, M. (2013) Molecular mechanisms of the PRL phosphatases. *FEBS J. 280*, 505−524.
(23) Kong, L., Li, Q., Wang, L., Liu, Z., and Sun, T. (2007) The value and correlation between PRL-3 expression and matrix metalloproteinase activity and expression in human gliomas. *Neuropathology 27*, 516−521.
(24) Campbell, A. M., and Zhang, Z. Y. (2014) Phosphatase of regenerating liver: A novel target for cancer therapy. *Expert Opin. Ther. Targets*, 1−15.
(25) Bardelli, A., Saha, S., Sager, J. A., Romans, K. E., Xin, B., Markowitz, S. D., Lengauer, C., Velculescu, V. E., Kinzler, K. W., and Vogelstein, B. (2003) PRL-3 expression in metastatic cancers. *Clin. Cancer Res. 9*, 5607−5615.
(26) Reich, R., Hadar, S., and Davidson, B. (2011) Expression and clinical role of protein of regenerating liver (PLR) phosphatases in ovarian carcinoma. *Int. J. Mol. Sci. 12*, 1133−1145.
(27) Park, H., Jung, S. K., Jeong, D. G., Ryu, S. E., and Kim, S. J. (2008) Discovery of novel PRL-3 inhibitors based on the structure-based virtual screening. *Bioorg. Med. Chem. 18* (7), 2250−2255.
(28) Guo, K., Tang, J. P., Jie, L., Al-Aidaroos, A. Q., Hong, C. W., Tan, C. P. B., Park, J. E., Varghese, L., Feng, Z., Zhou, J., Chng, W. J., and Zeng, Q. (2012) Engineering the first chimeric antibody in targeting intracellular PRL-3 oncoprotein for cancer therapy in mice. *Oncotarget 3* (2), 158−171.
(29) Al-Aidaroos, A. Q. O., and Zeng, Q. (2010) PRL-3 phosphatase and cancer metastasis. *J. Cell. Biochem. 111* (5), 1087−1098.
(30) Barford, D., Das, A. K., and Egloff, M. P. (1998) The structure and mechanism of protein phosphatases: Insights into catalysis and regulation. *Annu. Rev. Biophys. Biomol. Struct. 27*, 133−164.
(31) Bessette, D. C., Qiu, D., and Pallen, C. J. (2008) PRL PTPs: Mediators and markers of cancer progression. *Cancer Metastasis Rev. 27*, 231−252.
(32) Jain, J., Barford, D., Flint, A. J., and Tonks, N. K. (1995) Structural basis for phosphotyrosine peptide recognition by protein tyrosine phosphatase 1B. *Science 268*, 1754−1758.
(33) Schubert, H. L., Fauman, E. B., Stuckey, J. A., Dixon, J. E., and Saper, M. A. (1995) A ligand-induced conformational change in the *Yersinia* protein tyrosine phosphatase. *Protein Sci. 4*, 1904−1913.
(34) Brandão, T. A. S., Hengge, A. C., and Johnson, S. J. (2010) Insights into the reaction of protein-tyrosine phosphatase 1B crystal structures for transition state analogs of both catalytic steps. *J. Biol. Chem. 285* (21), 15874−15883.
(35) Kim, K. A., Song, J. S., Jee, J., Sheen, M. R., Lee, C., Lee, T. G., Ro, S., Cho, J. M., Lee, W., Yamazaki, T., Jeon, Y. H., and Cheong, C. (2004) Structure of human PRL-3, the phosphatase associated with cancer metastasis. *FEBS Lett. 565*, 181−187.
(36) Kozlov, G., Cheng, J., Ziomek, E., Banville, D., Gehring, K., and Ekiel, I. (2004) Structural insights into molecular function of the metastasis-associated phosphatase PRL-3. *J. Biol. Chem. 279*, 11882−11889.
(37) Swarup, G., Cohen, S., and Garbers, D. L. (1982) Inhibition of membrane phosphotyrosyl-protein phosphatase activity by vanadate. *Biochem. Biophys. Res. Commun. 107*, 1104−1109.
(38) Cole, R., and Loria, J. P. (2002) Evidence for flexibility in the function of ribonuclease A. *Biochemistry 41*, 6072−6081.
(39) Baldwin, A. J., and Kay, L. E. (2009) NMR spectroscopy brings invisible protein states into focus. *Nat. Chem. Biol. 5* (11), 808−814.
(40) Whittier, S. K., Whittier, S. K., Hengge, A. C., and Loria, J. P. (2013) Conformational motions regulate phosphoryl transfer in related protein tyrosine phosphatase. *Science 341*, 899−903.
(41) Delaglio, F., Grzesiek, S., Vuister, G. W., Zhu, G., Pfeifer, J., and Bax, A. (1995) NMRPipe: A multidimensional spectral processing system based on UNIX pipes. *J. Biomol. NMR 6*, 227−293.
(42) Goddard, T. D., and Kneller, D. G. (2008) *SPARKY 3*, University of California, San Francisco.
(43) Gütert, P., Mumenthaler, C., and Wührich, K. (1997) Torsion angle dynamics for NMR structure calculation with the new program DYANA. *J. Mol. Biol. 273*, 283−298.
(44) Shen, Y., Delaglio, F., Cornilescu, G., and Bax, A. (2009) TALOS+: A hybrid method for predicting protein backbone torsion angles from NMR chemical shifts. *J. Biomol. NMR 44*, 213−223.
(45) Chou, J. J., Gaemers, S., Howder, B., Louis, J. M., and Bax, A. (2001) A simple apparatus for generating stretched polyacrylamide gels, yielding uniform alignment of proteins and detergent micelles. *J. Biomol. NMR 21*, 377−382.
(46) Mulder, F. A. A., Skrynnikov, N. R., Hon, B., Dahlquist, F. W., and Kay, L. E. (2001) Measurement of slow (μs-ms) time scale dynamics in protein side chains by ^{15}N relaxation dispersion NMR spectroscopy: Application to Asn and Gln residues in a cavity mutant of T4 lysozyme. *J. Am. Chem. Soc. 123*, 967−975.
(47) Lipari, G., and Szabo, A. (1982) Model-free approach to the interpretation of nuclear magnetic resonance relaxation in macromolecules. 1. Theory and range of validity. *J. Am. Chem. Soc. 104*, 4546−4559.
(48) Lipari, G., and Szabo, A. (1982) Model-free approach to the interpretation of nuclear magnetic resonance relaxation in macromolecules. 2. Analysis of experimental results. *J. Am. Chem. Soc. 104*, 4559−4570.
(49) Cole, R., and Loria, J. P. (2003) FAST-Modelfree: A program for rapid automated analysis of solution NMR spin-relaxation data. *J. Biomol. NMR 26*, 203−213.
(50) Mandel, A. M., Akke, M., and Palmer, A. G., III (1995) Backbone dynamics of *Escherichia coli* ribonuclease HI: Correlations

with structure and function in an active enzyme. *J. Mol. Biol. 246*, 144−163.
(51) Palmer, A. G., III, Rance, M., and Wright, P. E. (1991) Intramolecular motions of azinc finger DNA-binding domain from Xfin characterized by proton-detected natural abundance ^{13}C heteronuclear NMR spectroscopy. *J. Am. Chem. Soc. 113*, 4371−4380.
(52) Tjandra, N., Feller, S. E., Pastor, R. W., and Bax, A. (1995) Rotational diffusion anisotropy of human ubiquitin from ^{15}N NMR relaxation. *J. Am. Chem. Soc. 117*, 12562−12566.
(53) Hiyama, Y., Niu, C.-H., Silverton, J. V., Bavoso, A., and Torchia, D. A. (1988) Determination of ^{15}N chemical shift tensor via $^{15}N-^{2}H$ dipolar coupling in Boc-glycylglycyl [^{15}N glycine] benzyl ester. *J. Am. Chem. Soc. 110*, 2378−2383.
(54) Fairbrother, W. J., Liu, J., Pisacane, P. I., Sliwkowski, M. X., and Palmer, A. G., III (1998) Backbone dynamics of the EGF-like domain of heregulin α. *J. Mol. Biol. 279*, 1149−1161.
(55) Agarwal, R., Burley, S. K., and Swaminathan, S. (2008) Structure of human dual specificity protein phosphatase 23, VHZ, enzyme-substrate/product complex. *J. Biol. Chem. 283*, 8946−8953.
(56) Rigas, J. D., Hoff, R. H., Rice, A. E., Hengge, A. C., and Denu, J. M. (2001) Transition state analysis and requirement of Asp-262 general acid/base catalyst for full activation of dual-specificity phosphatase MKP3 by extracellular regulated kinase. *Biochemistry 40*, 4398−4406.
(57) Jeong, D. G., Kim, S. J., Kim, J. H., Son, J. H., Park, M. R., Lim, S. M., Yoon, T. S., and Ryu, S. E. (2005) Trimeric structure of PRL-1 phosphatase reveals an active enzyme conformation and regulation mechanisms. *J. Mol. Biol. 345*, 401−413.
(58) Sun, J. P., Yang, W. Q., Yang, H., Liu, S., Liang, F., Fedorov, A. A., Almo, S. C., and Zhang, Z. Y. (2005) Structure and biochemical properties of PRL-1, a phosphatase implicated in cell growth, differentiation, and tumor invasion. *Biochemistry 44*, 12009−12021.
(59) Casey, P. J., and Seabra, M. C. (1996) Protein prenyltransferase. *J. Biol. Chem. 271*, 5289−5292.
(60) Grünler, J., and Parmryd, I. (1999) Subcellular distribution of farnesyl protein transferase in rat liver. *FEBS Lett. 455* (3), 233−237.
(61) Chi, Y., Kumar, T. K., Chiu, I. M., and Yu, C. (2000) ^{15}N NMR relaxation studies of free and ligand-bound human acidic fibroblast growth factor. *J. Biol. Chem. 275*, 39444−39450.
(62) Cole, R., and Loria, J. P. (2002) Evidence for flexibility in the function of ribonuclease A. *Biochemistry 41*, 6072−6081.
(63) Stone, M. J., Chandrasekhar, K., Holmgren, A., Wright, P. E., and Dyson, H. J. (1993) Comparison of backbone and tryptophan side-chain dynamics of reduced and oxidized *Escherichia coli* thioredoxin using ^{15}N NMR relaxation measurements. *Biochemistry 32*, 426−435.
(64) Bernado, P., Garcia de la Torre, J., and Pons, M. (2002) Interpretation of ^{15}N NMR relaxation data of globular proteins using hydrodynamic calculations with HYDRONMR. *J. Biomol. NMR 23*, 139−150.
(65) Yang, J., Liang, X., Niu, T., Meng, W., Zhao, Z., and Zhou, G. W. (1998) Crystal structure of the catalytic domain of protein-tyrosine phosphatase SHP-1. *J. Biol. Chem. 273*, 28199−28207.
(66) Pylypenko, O., Rak, A., Durek, T., Kushnir, S., Dursina, B. E., Thomae, N. H., Constantinescu, A. T., Anza Watzke, L. B., Waldmann, H., Goody, R. S., and Alexandrov, K. (2006) Structure of doubly prenylated Ypt1:GDI complex and the mechanism of GDI-mediated Rab recycling. *EMBO J. 25*, 13−23.
(67) Zeng, Q., Si, X., Horstmann, H., Xu, Y., Hong, W., and Pallen, C. J. (2000) Prenylation-dependent association of protein-tyrosine phosphatases PRL-1, -2, and -3 with the plasma membrane and the early endosome. *J. Biol. Chem. 275*, 21444−21452.
(68) Si, X., Zeng, Q., Ng, C. H., Hong, W., and Pallen, C. J. (2001) Interaction of farnesylated PRL-2, a protein-tyrosine phosphatase, with the β-subunit of geranylgeranyltransferase II. *J. Biol. Chem. 276*, 32875−32882.
(69) Wang, J., Kirby, C. E., and Herbst, R. (2002) The tyrosine phosphatase PRL-1 localizes to the endoplasmic reticulum and the mitotic spindle and is required for normal mitosis. *J. Biol. Chem. 277*, 46659−46668.
(70) Zeng, Q., Si, X., Horstmann, H., Xu, Y., Hong, W., and Pallen, C. J. (2000) Prenylation-dependent association of protein-tyrosine phosphatases PRL-1, -2, and -3 with the plasma membrane and the early endosome. *J. Biol. Chem. 275* (28), 21444−21452.
(71) Pascaru, M., Tanase, C., Vacaru, A. M., Boeti, P., Neagu, E., Popescu, I., and Szedlacsek, S. E. (2009) Analysis of molecular determinants of PRL-3. *J. Cell. Mol. Med. 13* (9B), 3141−3150.
(72) Sugase, K., Dyson, H. J., and Wright, P. E. (2007) Mechanism of coupled folding and binding of an intrinsically disordered protein. *Nature 447*, 1021−1025.
(73) Jeong, K. W., Jeong, M. C., Jin, B., and Kim, Y. (2013) Relationship between structural flexibility and function in the C-terminal region of the heparin-binding domain of $VEGF_{165}$. *Biochemistry 52* (49), 8823−8832.
(74) Lim, J., Sun, H., Fan, J. S., Hameed, I. F., Lescar, J., Liang, Z. X., and Yang, D. (2012) Rigidifying acyl carrier protein domain in iterative type I PKS CalE8 does not affect its function. *Biophys. J. 103* (5), 1037−1044.
(75) Jeong, K. W., Lee, J. Y., Lee, S. A., Yang, S. P., Go, H., Kang, D. I., Chae, C. B., and Kim, Y. (2011) Dynamics of a Heparin-Binding Domain of $VEGF_{165}$ Complexed with Its Inhibitor Triamterene. *Biochemistry 50*, 4843−4854.
(76) Mittermaier, A. K., and Kay, L. E. (2009) Observing biological dynamics at atomic resolution using NMR. *Cell 34*, 601−611.
(77) Krieger, F., Möglich, A., and Kiefhaber, T. (2005) Effect of proline and glycine residues on dynamics and barriers of loop formation in polypeptide chains. *J. Am. Chem. Soc. 127*, 3346−3352.
(78) Pellecchia, M., Sebbel, P., Hermanns, U., Wüthrich, K., and Glockshuber, R. (1999) Pilus chaperone FimC−adhesin FimH interactions mapped by TROSY-NMR. *Nat. Struct. Biol. 6*, 336−339.
(79) Koradi, R., Billeter, M., and Wüthrich, K. (1996) MOLMOL: A program for display and analysis of macromolecular structures. *J. Mol. Graphics 14*, 51−55.